Sensors and Actuators A 193 (2013) 87–94

Contents lists available at SciVerse ScienceDirect

Sensors and Actuators A: Physical

journal homepage: www.elsevier.com/locate/sna

Love mode surface acoustic wave ultraviolet sensor using ZnO films deposited on 36° Y-cut $LiTaO_3$

Hua-Feng Pang[a,b], Yong-Qing Fu[b,*], Zhi-Jie Li[a], Yifan Li[c], Jin-Yi Ma[d], Frank Placido[b], Anthony J. Walton[c], Xiao-Tao Zu[a,*]

[a] School of Physical Electronics, University of Electronic Science and Technology of China, Chengdu 610054, PR China
[b] Thin Film Centre, Scottish Universities Physics Alliance (SUPA), University of the West of Scotland, Paisley PA1 2BE, UK
[c] Institute for Integrated Micro and Nano Systems, Scottish Microelectronics Centre, School of Engineering, University of Edinburgh, Edinburgh EH9 3JF, UK
[d] Sichuan Institute of Piezoelectric and Acousto-optic Technology, Chongqing 400060, PR China

ARTICLE INFO

Article history:
Received 21 August 2012
Received in revised form 8 January 2013
Accepted 9 January 2013
Available online xxx

Keywords:
Ultraviolet sensor
Love mode SAW
ZnO film
Photoconductivity
Acoustic-electric interaction

ABSTRACT

Love mode surface acoustic wave (SAW) ultraviolet (UV) sensors were fabricated through sputtering ZnO films on 36° Y-cut $LiTaO_3$ substrate. Crystalline structure, morphology and photoluminescence (PL) of the sputtered ZnO films were characterized using X-ray diffraction, atomic force microscopy and fluorescence spectrometer. The PL spectra revealed that different defects in the ZnO films were dependent on the oxygen partial pressure during deposition. UV sensing measurements showed that at a power density of 350 $\mu W\,cm^{-2}$, the amplitude of the Love mode SAW UV sensor decreased up to −6.4 dB with a frequency shift of ~150 kHz under a 254 nm illumination. When this device was illuminated with 365 nm UV light at 570 $\mu W\,cm^{-2}$, the amplitude of the transmission signal decreased only −2.5 dB without any significant frequency shift. A frequency hopping effect during the downshift and recovery periods was identified due to the simultaneous interplays between the variations of the acoustic velocity and attenuation during the acoustic-electric interaction.

1. Introduction

Recently, ZnO-based surface acoustic wave (SAW) devices have attracted much interest in ultraviolet (UV) sensor, gas sensor, biosensor and microfluidics [1–5]. Semiconducting ZnO films with a wide bandgap of ~3.3 eV exhibit a good photoconductivity, and thus have been used to fabricate Schottky photodiodes, field-effect transistors, and SAW resonators for UV sensing applications [6–10]. ZnO-based SAW UV sensor possesses advantages of good passivity, low-cost, high reliability and good reproducibility [11]. ZnO films serving as a photo-conducting layer can be deposited on the SAW propagating path, and a good photo-response to the slight change in the acoustic-electric interaction arises from the variation of the sheet resistivity and carrier concentration in the ZnO film [12]. Changes in the velocity and amplitude of the SAW signal can be exploited to monitor the physical variation of the sensing layer, surface and interface of the multi-layers among sensing layers and piezoelectric substrates influenced by the wavelength and power density of the UV light.

For SAW UV sensing, the Rayleigh-mode SAW devices can be used to detect the acoustic-electric interaction, and the sensing mechanism have been explained [11,13–18]. Typical sensing layers such as GaN film or ZnO film have been deposited on the SAW devices and a frequency downshift of 60 kHz has been reported based on a GaN/sapphire SAW oscillator with a frequency of 200 MHz under UV irradiation in the wavelength range of 330–400 nm [13]. For another example, a 200 nm-thick ZnO film was sputter-deposited onto a $LiNbO_3$ SAW device operated at 37 MHz, which exhibited a large frequency shift of 170 kHz when illuminated using 365 nm UV light with an intensity of 40 $mW\,cm^{-2}$ [14]. Kumar et al. deposited a 71 nm-thick ZnO film on a $LiNbO_3$ SAW filter with an operating frequency of 37 MHz, which could detect a low-level intensity of 450 $nW\,cm^{-2}$ for the 365 nm UV light [15]. Furthermore, nanocystalline ZnO films with various morphologies of nanoparticles, nanorods and nanowires have been grown on the Rayleigh mode SAW devices to improve their photoconductivity [10,16–19]. Besides the fundamental Rayleigh mode, the Sezawa mode SAW has also been adopted to analyze the acoustic-electric effect [1,11]. Emanetoglu et al. introduced a Mg:ZnO layer in the ZnO/Mg:ZnO/ZnO/Si structure for the ZnO SAW filter, which exhibited a good sensitivity to a power density of 810 $\mu W\,cm^{-2}$ when operated using the Sezawa mode SAW of 711.3 MHz [1]. Wei et al. demonstrated that a large frequency

* Corresponding authors.
E-mail addresses: richard.fu@uws.ac.uk (Y.-Q. Fu), xtzu@uestc.edu.cn (X.-T. Zu).

0924-4247/$ – see front matter © 2013 Elsevier B.V. All rights reserved.
http://dx.doi.org/10.1016/j.sna.2013.01.016

shift of 1.017 MHz could be obtained for the 385 nm UV light at a power density of 551 μW cm^{-2} using the Sezawa mode SAW (with a frequency of 842.8 MHz) [11].

Love mode SAW is generated from a shear-horizontal acoustic wave propagating in a guiding layer on top of the piezoelectric substrate. SAW device in this mode possesses a good sensitivity to the mass change and photoconductivity variation for applications in liquid biosensing, gas sensing and photodetection [20–22]. Water et al. reported that a 1 μm-thick sputtered ZnO film on a 90° rotated ST-cut (42°45′) quartz SAW device did not generate any apparent response when illuminated with a 365 nm UV light, but ZnO nanorods grown on the ZnO/90° rotated ST cut (42°45′) quartz SAW device significantly enhanced the UV sensitivity [23]. Hence, the photoconductivity of ZnO films is related to their crystalline structure and defect properties, which can be varied by controlling the film growth conditions. Recent advances of the studies in semiconducting ZnO thin films also showed that the photoelectric properties are determined by the crystal quality and crystallization conditions on various substrates [24–28]. This enables the sensitivity of the Love mode SAW UV sensor to be optimized through sputtering the ZnO film on a shear-horizontal SAW device under appropriate growth conditions. However, rotated 90° ST-cut quartz has a low electromechanical coupling coefficient (k^2) of 0.11% and low dielectric constant of 4.5 [29,30]. Whereas, the 36° Y-cut $LiTaO_3$ possesses a large k^2 of 4.7% and high dielectric constant of 47, which is beneficial to improve the sensitivity of the Love mode SAW UV sensor [31]. To date, Love mode SAW UV sensor based on the ZnO/36° Y-cut $LiTaO_3$ structure has seldom been reported to detect the UV lights of different wavelengths and low power densities, and the related sensing mechanisms have not been clearly elucidated.

In this paper, ZnO/36° Y-cut $LiTaO_3$ SAW devices have been fabricated and characterized to study their UV light sensing capabilities based on different deposition conditions of the ZnO films. The real-time responses of amplitude and frequency of the Love mode SAW UV sensors have been measured as a function of UV light illumination intensity. UV sensing mechanism of the Love mode SAW device was investigated based on the analysis of acoustic-electric interaction.

2. Experimental

A 4 in. wafer of 36° rotated Y-cut $LiTaO_3$ was used as the piezoelectric substrate and standard lithography techniques was employed to pattern the inter-digital transducers (IDTs). The 150 nm thick aluminum IDTs consisted of 30 pairs of fingers with a wavelength of 100 μm and an aperture size of 2.5 mm. ZnO films were deposited on the surface of the SAW device using a direct current (DC) reactive magnetron sputter system (NS3750, Nordiko) and a 99.99% purity zinc target was used as the magnetron cathode. The distance of the sample from the target surface was about 10 cm and the chamber was pumped down to the base pressure of 2.0×10^{-3} Pa. The flow rates of the argon and oxygen gases were 90 and 45 sccm, respectively. Pre-conditioning of the target was performed for 20 min to clean and oxidize the surface of the zinc target to form a thin stable ZnO layer followed by a one hour deposition with a DC power of 400 W and a working pressure of 0.64 Pa. The substrate temperature was increased from 25 °C to 40 °C without substrate-heating treatment during the deposition. A second device with 30 pairs of fingers with a wavelength of 100 μm and aperture size of 1.5 mm was fabricated with a two hour deposition at a working pressure of 0.33 Pa and an oxygen partial pressure of 60%. The center frequencies of the Love mode devices were measured using an HP8752a network analyzer, which was ~41.5 MHz.

The ZnO films were characterized using X-ray diffraction (XRD, D5000, Siemens) with Cu Kα radiation (λ = 1.5406 Å). The thickness of the ZnO films was measured using a surface profiler (Veeco Dektak). Surface morphologies and roughness of the ZnO films were characterized using an atomic force microscope (AFM, CSPM4000, Ben-Yuan), and photoluminescence (PL) spectra were measured at room temperature using a fluorescence spectrometer (LS-55, Perkin-Elmer).

The ultraviolet light sensing was performed by illuminating the Love mode SAW device with a UV source of wavelengths ranging between 254 and 365 nm (UVGL-15, 4 W, UVP) at different optical power densities measured using an optical power meter. The real-time loop responses of the frequency and magnitude of the SAW devices to the ultraviolet light illumination were recorded every 4.6 s using a data acquisition system. The photocurrents of the ZnO films on the $LiTaO_3$ substrate were measured at room temperature in air using a Keithly 2400 digital source-meter through applying a DC voltage of 1 V on the IDT, illuminated by the UV light with different wavelengths and power densities for 1 min.

3. Results and discussions

3.1. Structure and morphology

Fig. 1a shows the surface profile of the two ZnO films deposited, which indicates that the thickness of the ZnO film deposited at the 0.64 Pa for one hour is ~1.39 μm, and that deposited at 0.33 Pa for 2 h is ~1.75 μm. The resulting thickness of the ZnO films on the $LiTaO_3$ substrate is near to or in the range of 1.2–1.5 μm in order to obtain a large value of k^2 for the ZnO/$LiTaO_3$ structure [22]. Fig. 1b shows the XRD patterns of the two samples. Only the (0 0 0 2) peak

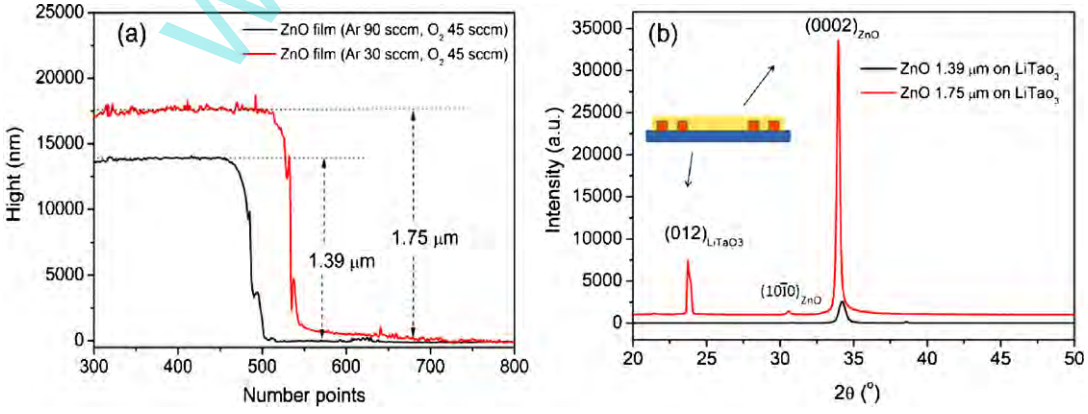

Fig. 1. (a) Step heights of sputtered ZnO films on 36° Y-cut $LiTaO_3$ SAW devices, (b) XRD patterns of ZnO films deposited on the 36° Y-cut $LiTaO_3$ SAW devices; the inset shows layer structure of ZnO/$LiTaO_3$ SAW device.

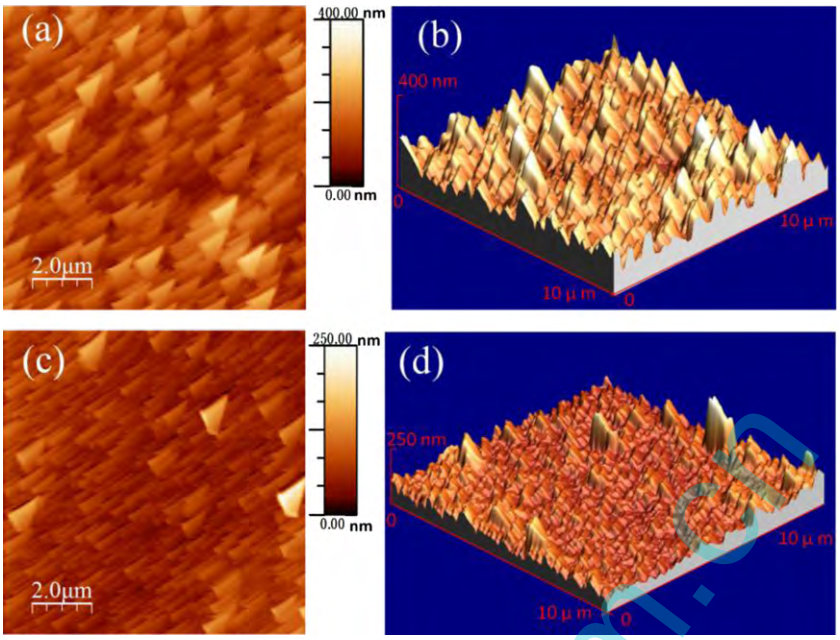

Fig. 2. AFM images of ZnO films deposited on the $LiTaO_3$ SAW devices with the thickness of (a, b) ~1.39 μm and (c, d) ~1.75 μm, respectively.

for the ZnO film and (0 1 2) peak for the $LiTaO_3$ substrate were observed indicating a highly textured ZnO films with a c-axis preferred orientation. The grain size was estimated using the Scherrer's formula with the removal of the equipment induced beam broadening, and found to be ~15.9 nm for the ~1.39 μm-thick ZnO film and ~31.2 nm for the ~1.75 μm ZnO film [32]. The peak shift of the film compared to the unstrained reference data of the bulk material indicates that the ZnO films were compressively strained. The strain ε in the ZnO films along *c*-axis is estimated by [33]

$$\varepsilon_{film} = \frac{c_{film} - c_{bulk}}{c_{bulk}} \quad (1)$$

where c_{film} is *c*-axis lattice constant of the films obtained from the position of the (0 0 0 2) peak, and c_{bulk} is the unstrained lattice parameter of the bulk ZnO taken as 0.52069 nm [33]. The strain is calculated to be 1.31% for the ~1.75 μm-thick ZnO film with a (0 0 0 2) diffraction peak at 33.96°. This is much larger than 0.45% for the ~1.39 μm-thick ZnO film with a (0 0 0 2) diffraction peak at 34.26°.

Fig. 2 shows the surface morphologies of the ZnO films on the 36° Y-cut $LiTaO_3$ SAW device. Fig. 2a shows the lateral feature of the ~1.39 μm-thick ZnO film as triangular-stacked shapes and the corresponding three-dimensional (3D) surface in Fig. 2b shows the tip-like microstructure, with a surface roughness of ~38.9 nm. Fig. 2c shows the surface feature of ~1.75 μm-thick ZnO film, which consists of rod-like shapes stacked horizontally with the occasional triangular structure, and a 3D AFM morphology presented in Fig. 2d shows a relatively smoother surface with a roughness of ~21.8 nm. Analysis of the XRD results and surface morphology suggests that the ~1.75 μm-thick ZnO film deposited at the oxygen partial pressure of 60% has a relatively denser microstructure than those of ~1.39 μm thick.

3.2. Photoluminescence property

It is known that defects in the nanocrystalline ZnO films play an important role on the photoelectric property of the ZnO films [7,9,11,23]. Fig. 3 shows the PL spectra of the ZnO films measured under Xe-lamp excitation of 325 nm at room temperature. The strong peaks at 385 and 400 nm of the emission spectra correspond to the near-band edge transition and zinc vacancy V_{Zn}, respectively [34,35]. This indicates that the ~1.75 μm-thick ZnO film deposited under a relatively higher oxygen partial pressure exhibits a better crystallinity. The ~1.39 μm-thick ZnO film, which was deposited under a lower oxygen partial pressure, displays a multi-peak PL structure that originates from different types of intrinsic defects. The peak at 424 nm is associated with the interstitial zinc [36], while the electron transition from a deep donor (oxygen vacancy) to the valence band are attributed to the origins of the 447 and 461 nm emissions [37]. The sharp peak at 486 nm is caused by the lattice defects related to oxygen vacancies and zinc vacancies, and the weak green emission peak at 529 nm is from singly-ionized oxygen vacancies on the surface [38,39]. The different defects observed in the ~1.39 μm-thick ZnO film suggest that the higher oxygen content of the working gas significantly reduces the formation of oxygen vacancies and zinc interstitial when the deposition rate is ~14.6 nm/min. In contrast, a relatively larger deposition rate of 23.2 nm/min and the lower oxidation efficiency of the target surface resulted in a zinc-rich sample due to the low oxygen partial pressure of 33.33% [40,41]. It can be concluded from the PL analysis that the defects of the ZnO films are altered by the deposition

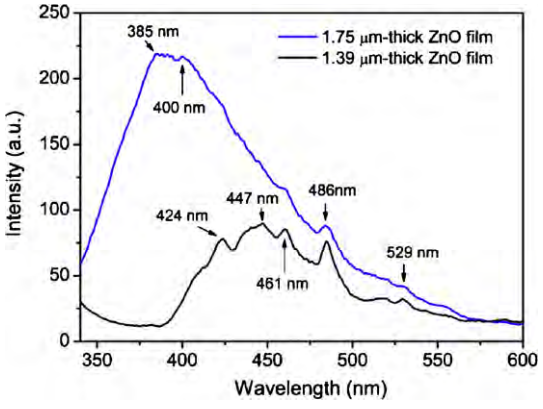

Fig. 3. Photoluminescence spectra of the ZnO films on the $LiTaO_3$ based SAW devices under different deposition parameters.

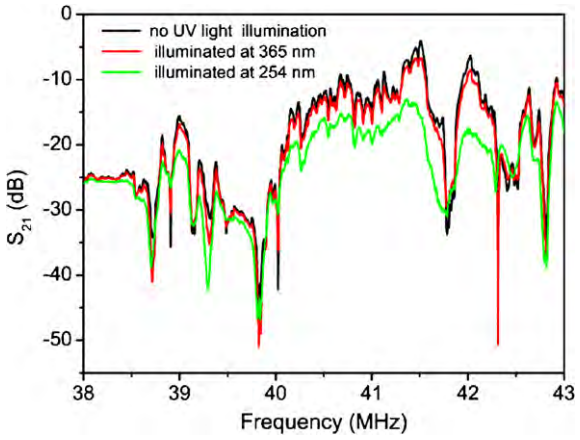

Fig. 4. Frequency responses (S_{21}) of the ZnO/$LiTaO_3$ SAW device under the UV light illumination at 254 nm with a power density of 0.71 mW cm^{-2} and at 365 nm with a power density of 0.57 mW cm^{-2}, respectively.

conditions, which certainly has a significant influence on the photoconductivity under the UV irradiation.

3.3. UV light sensing of the Love mode SAWs

The transmission signals of the Love mode SAW UV sensors were measured under a UV light illumination. Fig. 4 shows the frequency response (S_{21}) of the Love mode SAW UV sensors made from the ~1.39 μm-thick ZnO film. The frequency shift and decrease in the insertion loss were clearly observed when the device was illuminated using the UV light with wavelengths of 365 nm and 254 nm with power densities of 0.57 mW cm^{-2} and 0.71 mW cm^{-2}, respectively. The responses to the UV light with different wavelengths reveal that the defects in the ZnO film can trap the photons with different energies and generate electron–hole pairs. The free carriers in the guiding layer interact with the moving electric field from the SAW, resulting in the frequency shifts and the decreased magnitudes.

To investigate the sensing repeatability and stability, real-time responses of the frequency and magnitude of the UV sensor were recorded and the results of the UV light source being switched on and off for several exposure cycles are shown in Fig. 5. The maximum amplitude change of the SAW UV sensor with a ~1.39 μm-thick ZnO film was −12.5 dB, when illuminated using the 254 nm UV light at 2.17 mW cm^{-2}. Fig. 5a shows that the frequency response has a step change during the recovery to the initial value (see under the irradiation of the 254 nm UV light at 2.17 mW cm^{-2}), which consists of two frequency shifts of $\Delta f_1 = 50$ kHz and $\Delta f_2 = 100$ kHz. This frequency hopping effect is considered to be triggered by simultaneous interplays between the variations of the acoustic velocity and attenuation during the acoustic-electric interaction [12]. When this UV sensor is illuminated using the 365 nm UV light with a power density of 1.78 mW cm^{-2}, the maximum amplitude change is −5.3 dB. Only a frequency shift of ~50 kHz is observed in Fig. 5b without any apparent step during the downshift and recovery. It is possible that the photocurrent in this film is not large enough for the frequency hopping effect to occur. The subsequent loop response exhibits a good repeatability and stability. Fig. 6 shows the real-time response to UV light illumination of SAW UV sensor with a ~1.75 μm-thick ZnO film. There is only a very weak real-time response of the amplitude to the large optical power density (i.e. 3.85 mW cm^{-2} for the 254 nm UV light and 3.10 mW cm^{-2} for the 365 nm UV light), indicating that the acoustic-electric interaction has been slightly changed due to a small change of the sheet conductivity in the ZnO film. It can be concluded that the zinc vacancy V_{Zn} of the defects has a very weak contribution to the photoconductivity combining with the photoluminescence analysis.

In order to understand how the defects contribute to the photocurrents of ZnO films, the photo-current responses of the ZnO films on $LiTaO_3$ substrates were measured as shown in Fig. 7. Both the ZnO films with different deposition parameters exhibit photo responses when illuminated using the UV light with wavelengths of 254 and 365 nm, respectively. However, the decay process of the photocurrent in the ~1.39 μm ZnO film shows a much faster response than that in the ~1.75 μm ZnO film when the UV exposure is off. This indicates that generation mechanisms of the photocurrent may be different upon the UV illumination. For the ~1.39 μm ZnO film, the oxygen molecules chemisorbed on the grain boundary can diffuse into the boundary structures and fill up oxygen vacancies at the surface [42,43]. The adsorption of chemisorbed oxygen forms a high-resistance depletion layer at the surface resulting in a very small current in the ZnO film as shown in Fig. 7a. A lot of electron–hole pairs are generated and form a large photocurrent under the UV irradiation due to the significant decrease in the height of the barrier potentials. The current is quickly decayed to the initial value by recovering the chemisorptions of oxygen in the absence of the UV light [43,44]. The relatively lower resistance of the ~1.75 μm ZnO film originates from the excess donors of the ionized oxygen [45]. The longer decay time is related to a redistribution of surface ions and near-surface layer ions due to the high barriers of the relatively large grain [43]. The holes captured by deep traps at the grain boundaries slowly escape from the traps and recombine with free electrons, which results in a slow decrease in the conductivity and a difficult recovery of the initial state as the electron density drops [45,46].

A wide range of optical power densities were used to measure the amplitude change and frequency shift of the SAW UV sensor with a ~1.39 μm-thick ZnO film, and the results are shown in Fig. 8. Fig. 8a shows that the amplitude of the SAW sensor is

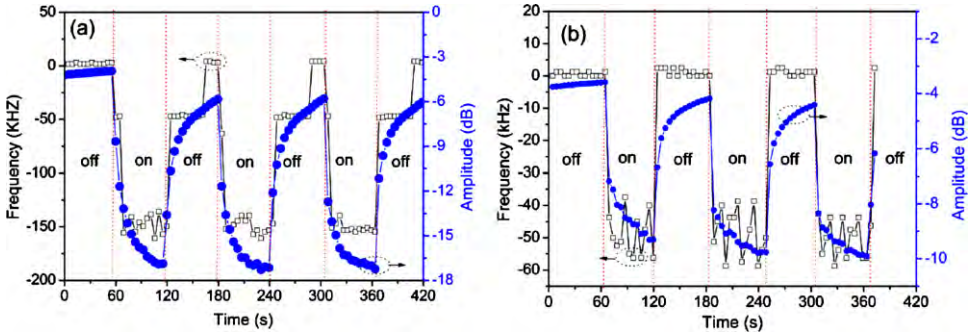

Fig. 5. Loop responses of the Love mode SAW UV sensor with a ~1.39 μm-thick ZnO film to the UV light (a) at 254 nm illuminated with a power density of 2.17 mW cm^{-2} and (b) at 365 nm illuminated with a power density of 1.78 mW cm^{-2}, respectively.

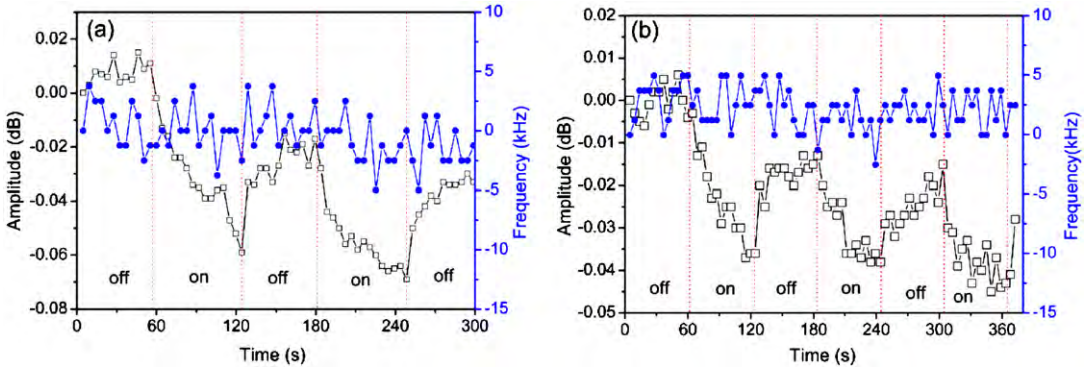

Fig. 6. Real-time responses of the Love mode SAW UV sensor with a ~1.75 μm-thick ZnO film to the UV light (a) at 254 nm illuminated with a power density of 3.85 mW cm^{-2} and (b) at 365 nm illuminated with a power density of 3.1 mW cm^{-2}, respectively.

significantly decreased under the illumination of the 254 nm UV light with power densities of 3.85–0.35 mW cm^{-2}. The response time reduces when the power density is decreased from 3.85 to 0.35 mW cm^{-2}. The maximum decrease in amplitude is ~16 dB for the 3.85 mW cm^{-2}. The amplitude changes indicate that the SAW UV sensor is sensitive to the power densities at a wavelength of the 254 nm. When the 365 nm UV light was switched from 0 to 3.10 mW cm^{-2}, the amplitude of the SAW UV sensor was increased from −3.7 to −13 dB as shown in Fig. 8b. The difference in the amplitude of the device is insignificant when the 365 nm UV light with a power density of 0.28 mW cm^{-2} was used. Clearly, the nature of the defect determines the concentration of the photo-generated carriers. The electron–hole pairs under photo-excitation are generated from the ionized oxygen defects in the grain boundaries and chemisorbed oxygen at the grain boundaries, and the photo-generated holes discharge with the negatively ionized oxygen releasing the chemisorbed oxygen, thus resulting in a photocurrent which has a linear response to the UV intensity [44,47,48]. The slow recovery to the initial amplitude could be assigned to the shallow traps created by zinc interstitials [47]. The difference of the amplitude responses with the UV wavelength could be explained due to the different photon-trapped abilities of the defects in the ZnO film [49,50].

Fig. 8c shows the total frequency shift (Δf) of ~150 kHz consisting of two sub-shifts ($\Delta f = \Delta f_1 + \Delta f_2$) with a step. It is interesting that the response time changes with different power densities of the 254 nm UV light, but the maximum frequency shifts have the same value of ~150 kHz. This is different compared with the conventional SAW UV sensors, which show apparent frequency shifts as the power density is modified. When the ZnO thickness is smaller than the acoustic wavelength, the velocity shift (ΔV) and the attenuation ($\Delta\Gamma$) from the acoustic-electric interaction can be estimated by [1,12,14]

$$\frac{\Delta V}{V_0} = -\frac{k^2}{2}\frac{\sigma_{sh}^2}{\sigma_{sh}^2 + V_0^2 C_s^2}, \tag{2}$$

$$\Delta\Gamma = \frac{k^2}{2}\frac{V_0 C_s \sigma_{sh}}{\sigma_{sh}^2 + V_0^2 C_s^2}, \tag{3}$$

where V_0, ΔV, k^2, C_s and σ_{sh} are the SAW velocity on free surface, SAW velocity difference, coupling coefficient, capacitance per unit length of the surface and the sheet conductivity of the ZnO film, respectively. This indicates that a small downshift of the frequency results in a decrease of the phase velocity, and the changes of amplitude correspond to SAW attenuation under the UV irradiation. However, the nearly constant value of the total frequency shift suggests that the sheet conductivity could approach a steady-state maximum value for the Love mode SAW UV sensor if illuminated for a sufficiently long time, which is different with the behavior of the Rayleigh mode SAW UV sensor [14–18]. The physical characteristic of the sheet conductivity is given by [1,12]

$$\sigma_{sh} = V_0 C_s = V_0[\varepsilon_1 + \varepsilon_2(\nu, t)], \tag{4}$$

where ε_1 and $\varepsilon_2(\nu,t)$ are the permittivities of the substrate and ZnO film, respectively. The permittivity of the ZnO film, $\varepsilon_2(\nu,t)$, changes with the wavelength and irradiation time of the UV light. The steady-state photoconductivity can quickly reach to a stable value when exposed to large optical power densities, but the photoconductivity relaxation is slow during the recovery process. When the wavelength of the UV light is changed to 365 nm, the appearance of the step in the downshift at a power density of 3.1 mW cm^{-2}

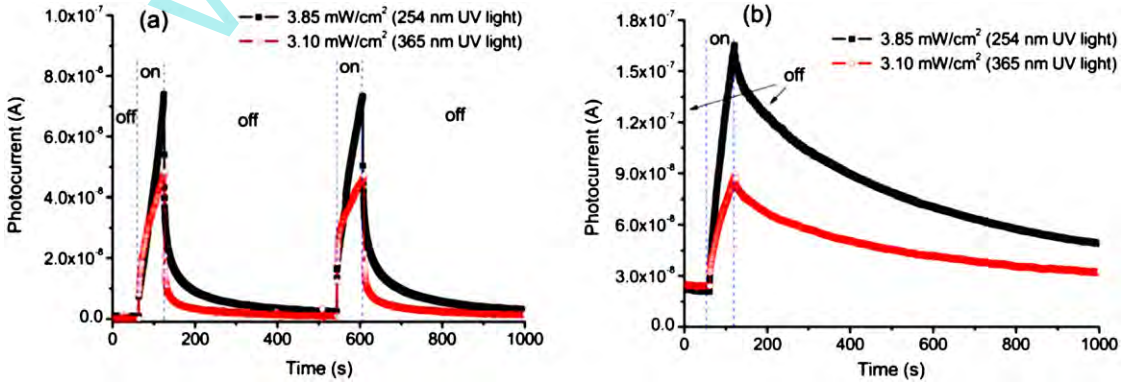

Fig. 7. Responses of the photocurrent of ZnO films with (a) a thickness of ~1.39 μm and (b) a thickness of ~1.75 μm, illuminated with different wavelengths and power densities.

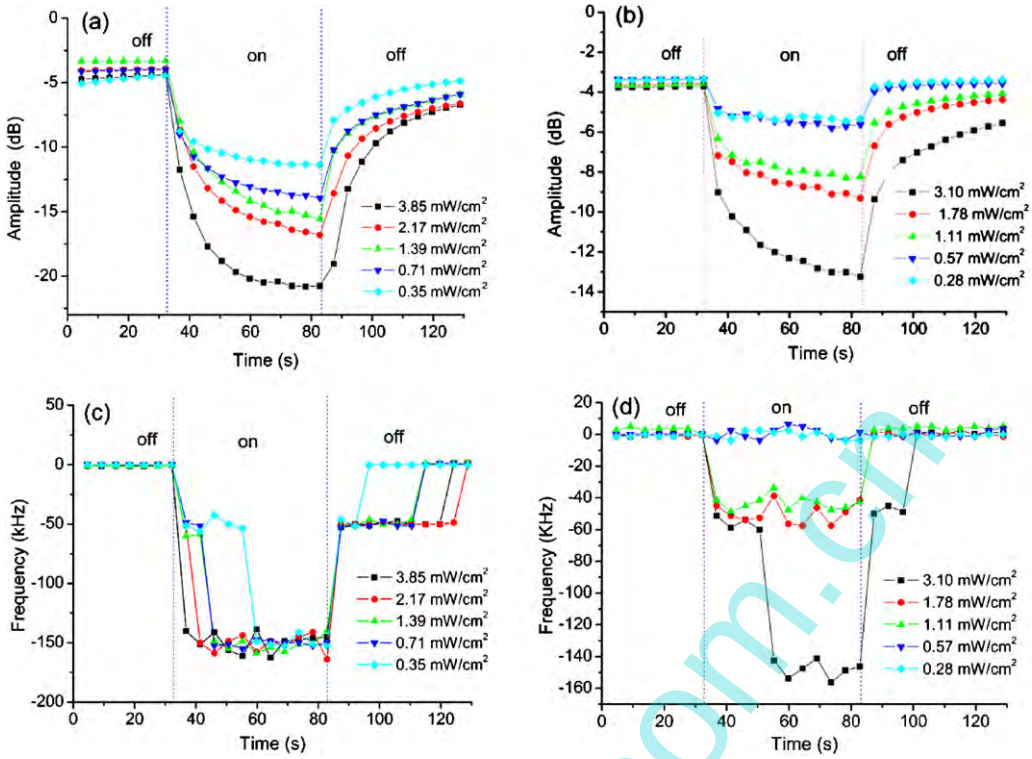

Fig. 8. Real-time amplitude change of the Love mode SAW UV sensor with a ~1.39 μm-thick ZnO film to the UV light at the wavelength of (a) 254 nm and (b) 365 nm under illumination with different power densities; real-time frequency response with the UV light at the wavelength of (c) 254 nm and (d) 365 nm under the illumination of different power densities.

indicates that the frequency hopping effect occurs only when the photo-excited carriers approach the saturation concentration in the acoustic-electric interaction as presented in Fig. 8d. The total frequency shift is about 150 kHz, which is similar to that obtained under irradiation with the 254 nm UV light. The change in sensitivity with the different wavelengths has been reported for the ZnO nanoparticles on $LiNbO_3$ SAW devices and was attributed the surface acceptor impurities [16]. Therefore, it is possible that the exposure using the UV light with different wavelengths results in the different concentrations of the photo-excited carriers due to the defect properties in the ZnO films even at the same optical power density.

Fig. 9a shows the amplitude change of the Love mode SAW UV sensor as a function of power density. The fitted curves indicate that the amplitude change exhibits an approximately linear relationship with the UV intensity, which has also been reported for a Rayleigh mode SAW oscillator designed to detect a 365 nm UV light [15]. This is attributed to the linear relation between the photocurrent in the ZnO film and power density of the UV irradiation [43,44]. As the power density is varied the maximum frequency shift remains an almost constant value of ~150 kHz for 254 nm illumination (see Fig. 9b), which means that the sheet conductivity could reach a maximum value at different UV intensities when the exposure time is long enough. However, the dependence of the frequency shift on the 365 nm UV intensity indicates that the sheet conductivity is influenced by the oxygen defects in the ZnO film, which exhibits monotonic variation before approaching the saturated concentration of the photo-excited carriers.

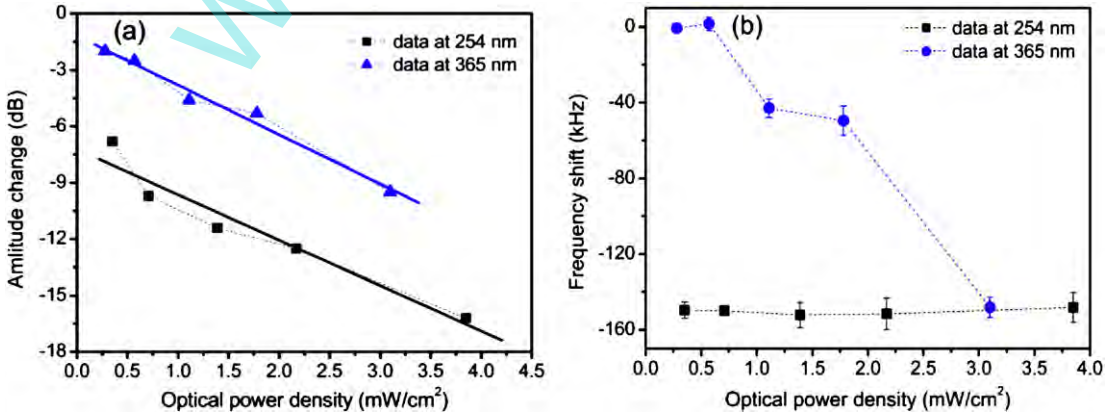

Fig. 9. (a) Amplitude change and (b) frequency shift of Love mode SAW UV sensor with a ~1.39 μm-thick ZnO film for the UV light at different optical power densities, the solid lines represent the linear fit.

4. Conclusions

Love mode surface acoustic wave ultraviolet sensors were fabricated using sputtered ZnO films on 36° Y-cut $LiTaO_3$ substrate and their thickness, crystalline structure, morphology and photoluminescence of the ZnO films were characterized using a surface profiler, X-ray diffraction, atomic force microscopy and fluorescence spectrometry. The PL spectra revealed that the different defects in the ZnO films were dependent on oxygen partial pressure during deposition. Results from the UV sensing measurements showed that the amplitude response of the Love mode SAW UV sensor operated at ~41.5 MHz changed up to −6.4 dB and the frequency shift approached ~150 kHz under a 254 nm illumination at the power density of 350 $\mu W\,cm^{-2}$. Whereas under a 365 nm illumination at 570 $\mu W\,cm^{-2}$, an amplitude of the transmission signal decreased only −2.5 dB with no significant frequency shift. The frequency hopping effect during the downshift and recovery periods was identified due to the simultaneous interplays between the variations of the acoustic velocity and attenuation during the acoustic-electric interaction.

Acknowledgements

This work was supported by the Fundamental Research Funds for the Central Universities (ZYGX2009J046 and ZYGX2009X007), the Sichuan Young Scientists Foundation (2010JQ0006), the Royal Society-Research Grant (RG090609), Carnegie Trust Funding, Royal Society of Edinburgh, Royal Academy of Engineering-Research Exchanges with China and India Awards and Scottish Sensor Systems Center (SSSC).

References

[1] N.W. Emanetoglu, J. Zhu, Y. Chen, J. Zhong, Y. Chen, Y. Lu, Surface acoustic wave ultraviolet photodetectors using epitaxial ZnO multilayers grown on r-plane sapphire, Applied Physics Letters 85 (2004) 3702–3704.
[2] A.Z. Sadek, W. Wlodarski, Y.X. Li, W. Yu, X. Li, X. Yu, K. Kalantar-zadeh, A ZnO nanorod based layered ZnO/64° YX $LiNbO_3$ SAW hydrogen gas sensor, Thin Solid Films 515 (2007) 8705–8708.
[3] K. Kalantar-Zadeh, W. Wlodarski, Y.Y. Chen, B.N. Fry, K. Galatsis, Novel Love mode surface acoustic wave based immunosensors, Sensors and Actuators B 91 (2003) 143–147.
[4] S. Krishnamoorthy, A.A. Iliadis, B. Thaleia, G.P. Chrousos, An interleukin-6 ZnO/SiO2/Si surface acoustic wave biosensor, Biosensors and Bioelectronics 24 (2008) 313–318.
[5] Y.Q. Fu, J.K. Luo, X.Y. Du, A.J. Flewitt, Y. Li, G.H. Markx, A.J. Walton, W.I. Milne, Recent developments on ZnO films for acoustic wave based bio-sensing and microfluidic applications: a review, Sensors and Actuators B 143 (2010) 606–619.
[6] L. Luo, Y.F. Zhang, S.S. Mao, L.W. Lin, Fabrication and characterization of ZnO nanowires based UV photodiodes, Sensors and Actuators A 127 (2006) 201–206.
[7] H. Kind, H.Q. Yan, B. Messer, M. Law, P.D. Yang, Nanowire ultraviolet photodetectors and optical switch, Advanced Materials 14 (2002) 158–160.
[8] H. Endo, M. Sugibuchi, K. Takahashi, S. Goto, S. Sugimura, K. Hane, Y. Kashiwaba, Schottky ultraviolet photodiode using a ZnO hydrothermally grown single crystal substrate, Applied Physics Letters 90 (2007) 121906.
[9] W. Kim, K.S. Chu, ZnO nanowire field-effect transistor as a UV photodetector: optimization for maximum sensitivity, Physica Status Solidi A 206 (2009) 179–182.
[10] S. Kumar, G.-H. Kim, K. Sreenivas, R.P. Tandon, ZnO based surface acoustic wave ultraviolet photo sensor, Journal of Electroceramics 22 (2009) 198–202.
[11] C.-L. Wei, Y.-C. Chen, C.-C. Cheng, K.-S. Kao, D.-L. Cheng, P.-S. Cheng, Highly sensitive ultraviolet detector using a ZnO/Si layered SAW oscillator, Thin Solid Films 518 (2010) 3059–3062.
[12] D. Dasgupta, K. Sreenivas, Frequency hopping due to acousto-electric interaction in ZnO based surface acoustic wave oscillator, Journal of Applied Physics 110 (2011) 044502.
[13] D. Ciplys, R. Rimeika, M.S. Shur, S. Rumyantsev, R. Gaska, A. Sereika, J. Yang, M. Asif Khan, Visible–blind photoresponse of GaN-based surface acoustic wave oscillator, Applied Physics Letters 80 (2002) 2020.
[14] P. Sharma, K. Sreenivas, Highly sensitive ultraviolet detector based on ZnO/LiNbO3 hybrid surface acoustic wave filter, Applied Physics Letters 83 (2003) 3617.
[15] S. Kumar, P. Sharma, K. Sreenivas, Low-intensity ultraviolet light detector using a surface acoustic wave oscillator based on ZnO/$LiNbO_3$ bilayer structure, Semiconductor Science and Technology 20 (2005) L27–L30.
[16] V. Chivukula, D. Ciplys, M. Shur, P. Dutta, ZnO nanoparticle surface acoustic wave UV sensor, Applied Physics Letters 96 (2010) 233512.
[17] T.-T. Wu, W.-S. Wang, T.-H. Chou, Y.-Y. Chen, Ultraviolet detector based on a surface acoustic wave oscillator system with ZnO-nanostructure sensing material, Journal of the Acoustical Society of America 123 (2008) 3377.
[18] W.S. Wang, T.T. Wu, T.H. Chou, Y.Y. Chen, A ZnO nanorod-based SAW oscillator system for ultraviolet detection, Nanotechnology 20 (2009) 135503.
[19] W. Peng, Y. He, C. Wen, K. Ma, Surface acoustic wave ultraviolet detector based on zinc oxide nanowire sensing layer, Sensors and Actuators A 184 (2012) 34–40.
[20] M.D. Schlensog, T.M.A. Gronewold, M. Tewes, M. Famulok, E. Quandt, A Love-wave biosensor using nucleic acids as ligands, Sensors and Actuators B 101 (2004) 308–315.
[21] N. Moll, E. Pascal, D.H. Dinh, J.-P. Pillot, B. Bennetau, D. Rebiere, D. Moynet, Y. Mas, D. Mossalayi, J. Pistre, C. Dejous, A Love wave immunosensor for whole *E. coli* bacteria detection using an innovative two-step immobilization approach, Biosensors and Bioelectronics 22 (2007) 2145–2150.
[22] S.J. Ippolito, A. Ponzoni, K. Kalantar-Zadeh, W. Wlodarski, E. Comini, G. Faglia, G. Sberveglieri, Layered WO3/ZnO/36(LiTaO3 SAW gas sensor sensitive towards ethanol vapour and humidity, Sensors and Actuators B 117 (2006) 442–450.
[23] W. Water, R.-Y. Jhao, L.-W. Ji, T.-H. Fang, S.-E. Chen, Love wave ultraviolet photodetector using ZnO nanorods synthesized on 90°-rotated ST-cut (42(45′) quartz, Sensors and Actuators A 161 (2010) 6–11.
[24] Y.-S. Choi, J.-W. Kang, D.-K. Hwang, S.-J. Park, Recent advances in ZnO-based light-emitting diodes, IEEE Transactions on Electron Devices 57 (2010) 26–41.
[25] J.W. Tomm, B. Ullrich, X.G. Qiu, Y. Segawa, A. Ohtomo, M. Kawasaki, H. Koinuma, Optical and photoelectrical properties of oriented ZnO films, Journal of Applied Physics 87 (2000) 1844.
[26] L.J. Mandalapu, F. Xiu, Z. Yang, J.L. Liu, Ultraviolet photoconductive detectors based on Ga-doped ZnO films grown by molecular-beam epitaxy, Solid-State Electronics 51 (2007) 1014–1017.
[27] M. Novotný, J. Čížek, R. Kužel, J. Bulíř, J. Lančok, J. Connolly, E. McCarthy, S. Krishnamurthy, J.-P. Mosnier, W. Anwand, G. Brauer, Structural characterization of ZnO thin films grown on various substrates by pulsed laser deposition, Journal of Physics D: Applied Physics 45 (2012) 225101.
[28] S.S. Shinde, K.Y. Rajpure, Fabrication and performance of N-doped ZnO UV photoconductive detector, Journal of Alloys and Compounds 22 (2012) 118–122.
[29] S.Y. Chu, W. Water, J.T. Liaw, An investigation of the dependence of ZnO film on the sensitivity of Love mode sensor in ZnO/quartz structure, Ultrasonics 41 (2003) 133–139.
[30] R.-C. Chang, S.-Y. Chu, C.-S. Hong, Y.-T. Chuang, A study of Love wave devices in ZnO/Quartz and ZnO/LiTaO3 structures, Thin Solid Films 498 (2006) 146–151.
[31] F.S. Hickernell, H.D. Knuth, R.C. Dablemont, T.S. Hickernell, The surface acoustic wave propagation characteristics of 64(Y-X $LiNbO_3$ and 36(Y-X $LiTaO_3$ substrates with thin-film SiO_2, Proceedings of the IEEE Ultrasonics Symposium (1995) 345–348.
[32] A.L. Patterson, The Scherrer formula for X-ray particle size determination, Physical Review 56 (1939) 978–982.
[33] X.Y. Li, H.J. Li, Z.J. Wang, H. Xia, Z.Y. Xiong, J.X. Wang, B.C. Yang, Effect of substrate temperature on the structural and optical properties of ZnO and Al-doped ZnO thin films prepared by dc magnetron sputtering, Optics Communication 282 (2009) 247–252.
[34] Z. Fang, Y. Wang, D. Xu, Y. Tan, X. Liu, Blue luminescent center in ZnO films deposited on silicon substrates, Optical Materials 26 (2004) 239–242.
[35] L. Yang, G. Wang, C. Tang, H. Wang, L. Zhang, Synthesis and photoluminescence of corn-like ZnO nanostructures under solvothermal-assisted heat treatment, Chemical Physics Letters 409 (2005) 337–341.
[36] B. Lin, Z. Fu, Y. Gia, Green luminescent center in undoped zinc oxide films deposited on silicon substrates, Applied Physics Letters 79 (2001) 943–945.
[37] A. Janotti, C.G. Van de Walle, Fundamentals of zinc oxide as a semiconductor, Reports on Progress in Physics 72 (2009) 126501.
[38] A.B. Djurisic, W.C.H. Choy, V.A.L. Roy, Y.H. Leung, C.Y. Kwong, K.W. Cheah, T.K. Gundu Rao, W.K. Chan, H.F. Lui, C. Surya, Photoluminescence and electron paramagnetic resonance of ZnO tetrapod structures, Advanced Functional Materials 14 (2004) 856–864.
[39] K. Vanheusden, W.L. Warren, C.H. Seager, D.R. Tallant, J.A. Voigt, B.E. Gnade, Mechanisms behind green photoluminescence in ZnO phosphor powders, Journal of Applied Physics 79 (1996) 7983–7990.
[40] S.-H. Jeong, B.-S. Kim, B.-T. Lee, Photoluminescence dependence of ZnO films grown on Si (100) by radio-frequency magnetron sputtering on the growth ambient, Applied Physics Letters 82 (2003) 2625–2627.
[41] Ü. Özgür, Y.I. Alivov, C. Liu, A. Teke, M.A. Reshchikov, S. Doğan, V. Avrutin, S.-J. Cho, H. Morkoc, A comprehensive review of ZnO materials and devices, Journal of Applied Physics 98 (2005) 041301.
[42] C. Soci, A. Zhang, B. Xiang, S.A. Dayeh, D.P.R. Aplin, J. Park, X.Y. Bao, Y.H. Lo, D. Wang, ZnO nanowire UV photodetectors with high internal gain, Nano Letters 7 (2007) 1003–1009.
[43] I.V. Tudose, P. Horváth, M. Suchea, S. Christoulakis, T. Kitsopoulos, G. Kiriakidis, Correlation of ZnO thin film surface properties with conductivity, Applied Physics A 89 (2007) 57–61.
[44] D.H. Zhang, Fast photoresponse and the related change of crystallite barriers for ZnO films deposited by RF sputtering, Journal of Physics D: Applied Physics 28 (1995) 1273–1277.

[45] J.N. Zeng, J.K. Low, Z.M. Ren, T. Liew, Y.F. Lu, Effect of deposition conditions on optical and electrical properties of ZnO films prepared by pulsed laser deposition, Applied Surface Science 197–198 (2002) 362–367.
[46] S.A. Studenikin, N. Golego, M. Cocivera, Optical and electrical properties of undoped ZnO films grown by spray pyrolysis of zinc nitrate solution, Journal of Applied Physics 83 (1998) 2104–2111.
[47] P. Sharma, K. Sreenivas, K.V. Rao, Analysis of ultraviolet photoconductivity in ZnO films prepared by unbalanced magnetron sputtering, Journal of Applied Physics 93 (2003) 3963.
[48] S. Kumar, G.-H. Kim, K. Sreenivas, R.P. Tandon, Mechanism of ultraviolet photoconductivity in zinc oxide nanoneedles, Journal of Physics: Condensed. Matter 19 (2007) 472202.
[49] Q.H. Li, T. Gao, Y.G. Wang, T.H. Wang, Adsorption and desorption of oxygen probed from ZnO nanowire films by photocurrent measurements, Applied Physics Letters 86 (2005) 123117.
[50] M.E. Swanwick, S.M.-L. Pfaendler, A.I. Akinwande, A.J. Flewitt, Near-ultraviolet zinc oxide nanowire sensor using low temperature hydrothermal growth, Nanotechnology 23 (2012) 344009.

Biographies

Hua-Feng Pang obtained his B.S. degree in School of Physics and Electronic Engineering, Nanyang Normal University, China in 2005. He is a Ph.D. student in School of Physical Electronics at University of Electronic Science and Technology of China. His present interests include applications of nanomaterials and functional thin films for sensors and microfluidic devices.

Richard Yong-Qing Fu received his Ph.D. degree from Nanyang Technological University, Singapore in 1999, and then worked in University of Cambridge and Heriot-Watt University, UK. He is a Reader in Thin Film Centre in University of the West of Scotland. His recent research has been focusing on microactuators, microsensors and microfluidic devices based on smart functional thin films.

Zhi-Jie Li received his Ph.D. degree from Institute of Coal Chemistry, Chinese Academy of Sciences in 2005. He is an associate professor in School of Physical Electronics at University of Electronic Science and Technology of China. His current interests are nanomaterials, novel functional materials and their spectroscopy.

Yi-Fan Li obtained his Ph.D. degree in School of Engineering and Electronics, the University of Edinburgh, UK, in 2007. He has been working in various MEMS areas in the past 5 years. During his Ph.D. study, he won the best presentation award in PREP2005 (IEEE & EPSRC). His current interest is microfluidic systems such as electro-wetting on dielectrics and surface acoustic wave, and bio-MEMS.

Jin-Yi Ma received his Ph.D. degree from Tianjin University in 2003. He is a senior research fellow in Sichuan Institute of Piezoelectric and Acousto-optic Technology. His research area is on piezoelectric materials and industrial applications of the acoustic-optical device.

Frank Placido obtained his Ph.D. degree from University of Edinburgh in 1973. He is a professor and director of thin film center in University of the West of Scotland. His research has been focused in the area of thin film coatings, particularly in their industrial applications and knowledge transfer, but also including fundamental research into plasmas and materials.

Anthony J. Walton is a professor of Scottish Microelectronics Centre in the School of Engineering at the University of Edinburgh. Over the past 25 years, he has been actively involved with the semiconductor industry in a number of areas associated with silicon processing which includes both IC technology and micro-systems. His present interests include the applications of micro and nanotechnology to biotechnology, organometallic materials for semiconductor applications, sensors and interconnect technology.

Xiao-Tao Zu received his Ph.D. degree from Sichuan University in 2002. He is a professor in School of Physical Electronics at University of Electronic Science and Technology of China. His research interests include photoelectric materials, smart materials, composite nano materials and their industrial applications.